ACS Energy LETTERS

http://pubs.acs.org/journal/aelccp

PERSPECTIVE

Lead Halide Perovskite Nanocrystals in the Research Spotlight: Stability and Defect Tolerance

He Huang,[†] Maryna I. Bodnarchuk,[∥,⊥] Stephen V. Kershaw,[†] Maksym V. Kovalenko,*[,∥,⊥] and Andrey L. Rogach*[,†]

[†]Department of Materials Science and Engineering and Centre for Functional Photonics (CFP), City University of Hong Kong, Kowloon, Hong Kong SAR

[∥]Institute of Inorganic Chemistry, Department of Chemistry and Applied Biosciences, ETH Zürich, CH-8093 Zürich, Switzerland

[⊥]Laboratory for Thin Films and Photovoltaics, Empa − Swiss Federal Laboratories for Materials Science and Technology, Überlandstrasse 129, CH-8600 Dübendorf, Switzerland

ABSTRACT: This Perspective outlines basic structural and optical properties of lead halide perovskite colloidal nanocrystals, highlighting differences and similarities between them and conventional II−VI and III−V semiconductor quantum dots. A detailed insight into two important issues inherent to lead halide perovskite nanocrystals then follows, namely, the advantages of defect tolerance and the necessity to improve their stability in environmental conditions. The defect tolerance of lead halide perovskites offers an impetus to search for similar attributes in other related heavy metal-free compounds. We discuss the origins of the significantly blue-shifted emission from $CsPbBr_3$ nanocrystals and the synthetic strategies toward fabrication of stable perovskite nanocrystal materials with emission in the red and infrared parts of the optical spectrum, which are related to fabrication of mixed cation compounds guided by Goldschmidt tolerance factor considerations. We conclude with the view on perspectives of use of the colloidal perovskite nanocrystals for applications in backlighting of liquid-crystal TV displays.

In the past few years, lead halide perovskites (LHPs) in the form of colloidal nanocrystals (NCs), such as organic−inorganic $CH_3NH_3PbX_3$ LHPs (often denoted as $MAPbX_3$, with MA standing for the methylammonium cation) and all-inorganic $CsPbX_3$ LHPs (X = Cl, Br, I), have been intensively investigated for various applications such as light-emitting devices (LEDs) and photodetectors due to their color-tunable and narrow-band emission as well as easy synthesis, convenient solution-based processing, and low fabrication cost. We refer interested readers to some recent reviews for comprehensive treatment of these topics.[1−6] Most striking has been the impact of thin-film perovskites in photovoltaics,[7] with extremely high power conversion efficiencies of more than 22%,[8] and the reports of light-emitting diodes with external quantum efficiencies over 10%.[9,10] The literature underpinning the development in bulk and thin-film perovskites is very extensive and is not covered herein; instead, we focus on nanoscale perovskite NCs and their emerging applications. In this Perspective, we first provide some short historical remarks on LHPs and then outline their basic structural and optical properties, highlighting differences and similarities between the LHP NCs and conventional II−VI and III−V semiconductor quantum dots (QDs). We then proceed with more detailed insight into two important issues inherent to LHP NCs, namely, the innate advantage of so-called defect tolerance and the necessary steps required to improve their stability under the environmental conditions found in devices. We then discuss several issues that need to be addressed in the burgeoning field of LHP NCs, such as the origin of the significantly blue-shifted photoluminescence (PL) from $CsPbBr_3$ NCs and the synthetic strategies toward fabrication of stable mixed-cation LHP NC materials with an optimum Goldschmidt tolerance factor (TF) that emit in the red and near-infrared part of the optical spectrum. The defect tolerance of LHP NCs offers strong inspiration to search for similar attributes in other related compounds, especially those that do not contain toxic lead or other heavy metals. We also provide our view on the perspectives on the use of the colloidal LHP NCs for applications in backlighting of liquid-crystal displays for

Received: June 26, 2017
Accepted: August 10, 2017
Published: August 10, 2017

DOI: 10.1021/acsenergylett.7b00547
ACS Energy Lett. 2017, 2, 2071−2083

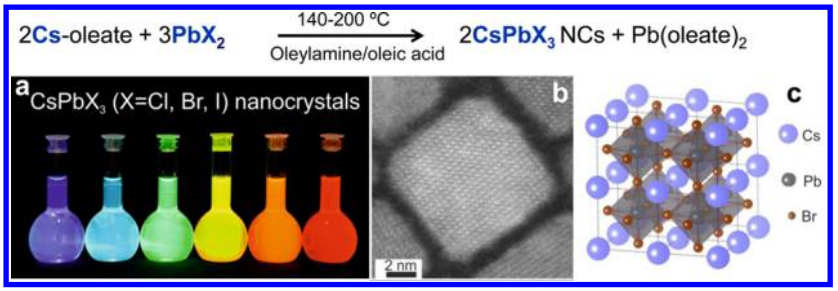

Figure 1. Colloidal synthesis of $CsPbX_3$ NCs and (a) photographs of resulting colloidal solutions of $CsPbX_3$ NCs; (b) HAADF-STEM image of a single $CsPbBr_3$ NC; (c) idealized perovskite crystal structure with 3D interconnection of PbX_6 octahedra. In reality, all $APbX_3$ perovskites not only adopt the cubic polymorph but are commonly observed in lattices with lower symmetry, for example, orthorhombic and tetragonal, due to distortions along one or more Pb−X−Pb axes. Adapted from refs 35 and 112.

television (LCD TV displays) and other related color conversion and color enhancement applications.

Basic Properties of Lead Halide Perovskite Nanocrystals. The synthesis of bulk $CsPbX_3$ compounds was reported as early as 1893,[11] whereas their perovskite crystal structure and photoconductive, and hence semiconductive, nature was only discerned later, in the 1950s.[12] Since then and until the late 1990s, $CsPbX_3$ compounds were rather thoroughly characterized as to the details of their crystallography and phase diagrams, including direct structural characterization by X-ray and neutron scattering and by nuclear magnetic resonance.[13−28] Also, a number of lead-free halide perovskites were studied at that time; $CsSnX_3$ phase transitions were characterized,[6,29−31] and specific electrical conductivity was observed.[32] $CsGeCl_3$ was reported to have dielectric constants comparable to $BaTiO_3$ while exhibiting ferroelectric characteristics as well.[33] In 1978, Weber et al. synthesized and determined the crystal structure of $MAPbX_3$ for the first time.[34]

The motivation to investigate LHPs in the form of colloidal NCs has its roots in prior successes of colloidal QDs of conventional semiconductors (CdSe, CdTe, PbSe, InP, and the like).[36] LHP NCs have spurred intense research efforts owing to, on one hand, their extremely facile synthesis (Figure 1, upper part) and, on the other hand, their very bright PL covering the entire visible spectral range (Figure 1a). These highly crystalline, cubic-shaped NCs (Figure 1b) reflect the intrinsic near-cubic symmetry of the crystal lattice (Figure 1c). Just like their perovskite oxide ancestors (i.e., $CaTiO_3$), LHPs crystallize into an ABX_3-like lattice that comprises three-dimensional (3D) corner-shared $[PbX_6]$ octahedra (X being Cl, Br, I). There are commonly three cations, namely, cesium (Cs^+), methylammonium (MA, $CH_3NH_3^+$), and formamidinium (FA, $CH(NH_2)_2^+$), which fit into a 12-coordinate A-site formed in between $[PbX_6]$ octahedra. According to the Goldschmidt TF,[37] any substantially larger or smaller, for example, by 10% or more, A-site ion would destabilize the lattice and induce conversion into lower-dimensional lead halide compounds, with much larger bandgaps, as was observed experimentally.[38]

Lead halide perovskites are highly ionic compounds.

In contrast to other semiconductor materials (Si, GaAs, Cd chalcogenides, In pnictides), LHPs are highly ionic compounds. Hence, it is not surprising that they readily and easily form highly crystalline NCs even at room temperature. Colloidal synthesis of $CsPbX_3$ NCs, depicted in Figure 1,[35] represents just one out of numerous variations of the ionic coprecipitation method, optimized to obtain narrow size dispersions. Size control and colloidal stability are imparted by the capping ligands, typically a mixture of a carboxylic acid (such as oleic acid, OA) and alkylamines (such as oleylamine, OLA).[39−42]

The first colloidal synthesis of organic−inorganic $MAPbBr_3$ NCs was reported in 2014 by Galian and Perez-Prieto, who used an alkyl ammonium bromide with a medium-sized chain to stabilize small-sized crystallites in a suspension;[43] the same group further enhanced their PL quantum yield (QY) to 100%.[44] Soon after that first publication, Zhong's group introduced a ligand-assisted reprecipitation (LARP) technique (as shown in Figure 2a) in a mixture of a good and a poor solvent to produce $MAPbX_3$ (X = Cl, Br, I) NCs with a tunable bandgap by varying halide elements; the same group also reported improved LARP and in situ fabrication later.[39,45−47] Later in Huang's related report,[40] bandgap tunability of $MAPbBr_3$ NCs while controlling the LARP process by modifying the poor solvent's temperature was demonstrated (Figure 2b), and NCs with high PL QYs of up to 93% and high crystallinity (Figure 2c) were obtained. 1D and 2D perovskite NCs have also been explored, and quantum confinement has been completely verified and quantified in the 2D case.[41,42,48] Simple top-down fabrication of $MAPbBr_3$ and $MAPbI_3$ NCs by employing a mixture of OA and OLA ligands as coordinating solvents under ultrasonication was also demonstrated by Huang et al.[49] The ultrasonication approach was also demonstrated by Hintermay et al. and Tong et al.[50,51]

Combinations of LHP NCs can provide wide color gamuts covering the whole visible spectral range (400−700 nm with $CsPbX_3$ and $MAPbX_3$ NCs) and the emission can even be extended into the infrared (up to 800 nm with $FAPbI_3$ NCs). In the visible, emission line widths are narrow, typically less than 100 meV, corresponding to a full width at half-maximum (fwhm) of 12−50 nm. The lower widths are seen at shorter wavelengths, in the blue, and a meaningful means of comparison is to take the fwhm divided by the central wavelength (i.e., the fractional bandwidth)[52] as this would bear some relationship to the size distribution and highlight major differences in the latter where the fractional bandwidths differ significantly. PL QYs are high, even without the benefits of core−shell passivation, and can reach peak values of up to 95−100%.[35,53] Such high PL QYs are a direct consequence of the defect-tolerant nature of LHP's electronic structure, which we will consider in detail below.

These attractive optical characteristics of LHP NCs are counterbalanced by several major issues related to the stability

DOI: 10.1021/acsenergylett.7b00547
ACS Energy Lett. 2017, 2, 2071−2083

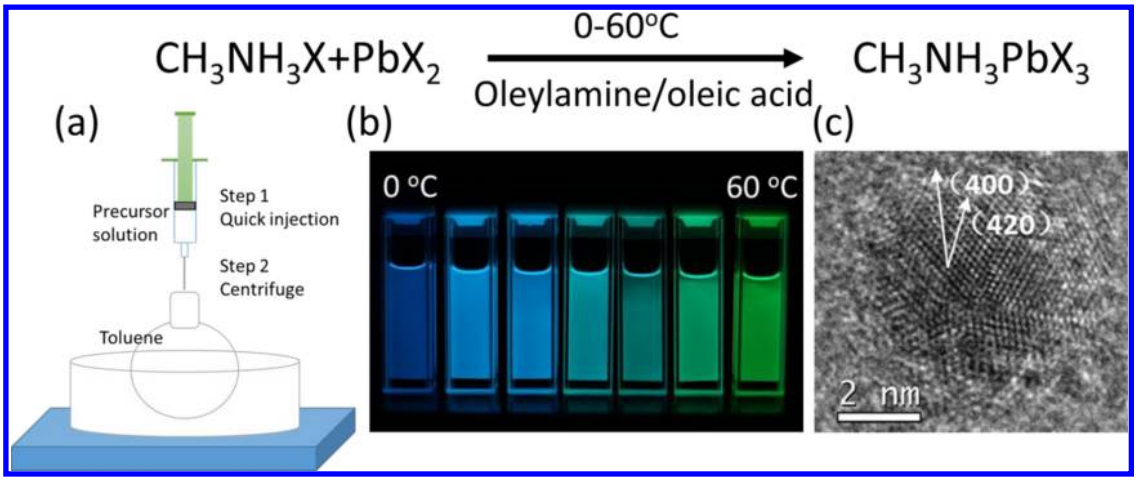

Figure 2. Colloidal synthesis of $MAPbBr_3$ NCs and (a) schematic diagram of the LARP reaction system; (b) colloidal solutions of $MAPbBr_3$ NCs obtained by using different temperatures of toluene solvent; (c) HRTEM image of a single $MAPbBr_3$ NC. Adapted from ref 40. Copyright 2015, Wiley Online Library.

of these materials. The key difficulty from the viewpoint of chemical stability concerns $MAPbX_3$ NCs.[43] Due to the low energy of formation, MA-based LHPs can eventually decompose into PbX_2 and volatile byproducts (i.e., CH_3NH_2, HI, I_2, etc.). This decomposition is greatly accelerated by the high surface area of LHP NCs and by moisture, oxygen, heat, light, and their combined effects.[54,55] Often, MA-based LHP NCs decompose during isolation and purification procedures. Higher durability has been observed with FA- and Cs-based LHP NCs.[35,53] Owing to the considerable ionicity of the bonding, yet another challenge specific to all LHP NCs is their instability in essentially all polar solvents. In addition, LHP NCs exhibit rather moderate thermal stability due to either low melting points of 400−500 °C ($CsPbX_3$) or thermal decomposition ($MAPbI_3$ at ca. 150−200 °C; $FAPbI_3$ at ca. 290−300 °C). In addition, a great challenge originates from the rather labile and dynamic nature of the ligand binding in these materials,[56] causing a loss of colloidal stability during the purification of LHP NC colloids. These challenges have led to intense research into alternative ligand chemistries[57,58] and developing coatings with protective polymeric or inorganic layers,[59,60] which we will consider in detail below.

Another form of structural instability comes from the polymorphism, which is especially pronounced for iodide-based LHPs ($CsPbI_3$ and $FAPbI_3$). 3D polymorphs of $CsPbI_3$ and $FAPbI_3$ are thermodynamically metastable and undergo transitions to wide-bandgap 1D polymorphs.[13−16,61−65] Thin films and NCs of $CsPbI_3$ and $FAPbI_3$ exhibit extended but finite stability in their 3D polymorphs (days to several months), primarily due to surface effects.[35,53,66−69] Thermodynamic instability is caused by the Cs and FA ions being, respectively, slightly too small and too large for the A-site, as determined by the Goldschmidt TF and by the octahedral factor for the required dense packing in 3D perovskites.[37,70−74] Combined with the chemical instability of the $MAPbI_3$ NC system, a "red wall" exists for LHP NCs—a difficulty to obtain stable NCs with PL in red and near-infrared spectral regions.

$APbX_3$ perovskites that feature 3D interconnection of PbX_6 octahedra are of primary interest. These octahedra form either an ideal cubic lattice (typical for $FAPbBr_3$ and $FAPbI_3$) or a similar 3D orthorhombic one ($CsPbX_3$). In the case of iodide LHPs ($FAPbI_3$ and $CsPbI_3$), 3D -phases are metastable at room temperature, and the instability decreases upon reduction of crystallite size from bulk to NCs.[53,75] Although $FAPbI_3$ NCs are stable for at least several months, $CsPbI_3$ NCs are highly unstable and, at best, retain their red PL for several weeks, only. Poor chemical stability of $MAPbI_3$ and poor phase stability of its FA and Cs cousins had been previously termed by us as the "perovskite red wall".[53] To illustrate the mitigation strategy on this issue, which can be based on employment of mixed-cation perovskites, we briefly review the underlying reasons for the phase transformation illustrated in Figure 3. Perovskite

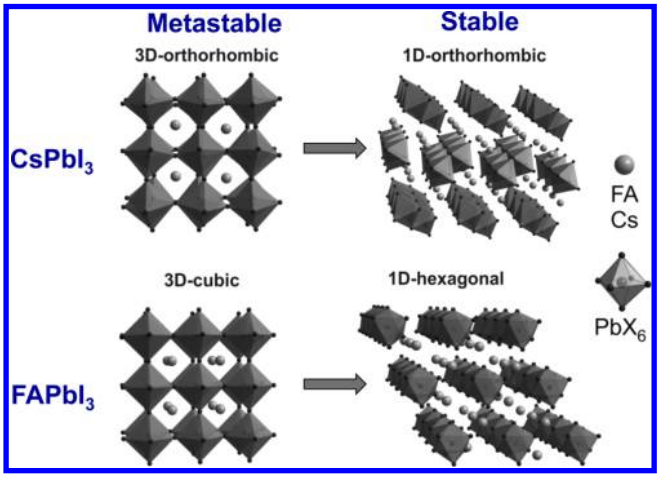

Figure 3. Illustration of the "perovskite red wall": 3D phases of $CsPbI_3$ (orthorhombic) and $FAPbI_3$ (pseudocubic) materials, with bandgap energies at ca. 710 and 840 nm, respectively, easily convert into wide-bandgap 1D polymorphs. The transition is typically observed as a change of the color from dark-red/black to yellow.

structures can be viewed as a close-packing of ions, and hence, the Goldschmidt TF concept, commonly used for metal-oxide perovskites[37] can be also extended to LHPs.[71,72] For ideal 3D cubic close-packing, the Goldschmidt TF is calculated as

$$\mathrm{TF} = \frac{(r_A + r_X)}{\sqrt{2}\,(r_{Pb} + r_X)}$$

where r_A, r_{Pb}, and r_X are the ionic radii of each ion. In an ideal close-packing case, TF = 1. Although for more ionic oxides TF

DOI: 10.1021/acsenergylett.7b00547
ACS Energy Lett. 2017, 2, 2071−2083

= 0.8−1 is known as an empirical stability range, higher covalency in LHPs and nonsphericity of their A-cations (both MA and FA) lead to the observation of stable 3D perovskites only for TF ≥ 0.9. The data from Travis et al.[71] for $APbX_3$ compounds provides TF values for $CsPbBr_3$ of 0.9 and for $CsPbI_3$ of 0.89, indicating that $CsPbI_3$ is likely a borderline case. In $FAPbI_3$, the nonsphericity of the cation complicates the analysis. Travis et al. estimated a radius of 2.53 Å for the FA cation, and the corresponding TF value for $FAPbI_3$ is 1.03. Cs−FA mixed-cation perovskites with composition-averaged TF values fall within the stability window, as demonstrated recently.[53,76] Similar strategies of the use of mixed-cation perovskite thin films have also led to major recent advances in photovoltaics, as demonstrated on $Cs_{0.17}FA_{0.83}(PbI_{1-x}Br_x)_3$ (x = 0−1), $(FAPbI_3)_{1-x}(MAPbBr_3)_x$ (x = 0−0.3), and (Cs/MA/FA/Rb)$(PbI_{1-x}Br_x)_3$.[77−81]

The tunability of perovskite nanocrystal compositions can be achieved after synthesis through subsequent anion exchange, which is more facile than that for many conventional II−VI and III−V quantum dots.

The composition control of LHP NCs is more flexible and convenient than that for many conventional semiconductor QDs. The tunability of perovskite NC compositions can be achieved after synthesis through subsequent anion exchange, which is more facile than that for many conventional II−VI and III−V QDs. In chalcogenide NCs, cation exchange is quite common and easy to certain degrees;[82] however, the anion exchange is rarely reported in such materials. Anion sublattice bonding is rather stronger than that of the cation sublattice, while the anions themselves are often bulkier than the cations, making anion exchange difficult without using extreme conditions, and usually any exchange that is observed is not topotaxial.[83,84]

Another outstanding feature of perovskite NCs is that they can have high PL QYs, which have even reached 100%,[44] by virtue of their fortuitous band structures, as discussed further in the next section. The PL fwhm of perovskite NCs is narrower than that for most of the other types of QDs.[1,35,36,39] Narrower line width emission is said to be more saturated, placing the fluorescence color coordinates more toward the curved edge of the CIE chromaticity space (e.g., CIE 1931 standard).[39,85] Combinations of three emitters (red, green, and blue), which lie close to the fully saturated boundary curve, can then create the widest range of perceived colors, termed the color gamut, by display and lighting manufacturers. The cost of production of perovskite NCs is regarded as low because of their solvent processing and relatively low temperature synthesis.

The relatively low or nonoccurrence of fluorescence blinking[86,87] of LHP NCs is an attractive prospect for hot carrier/multiexciton effects as it is probably a marker for relatively weak Auger recombination effects. However, the photothermal stability of the materials under high photon energy and at high fluences is a factor that needs to be addressed in order to fully realize the benefits of such effects.

Defect Tolerance of Lead Halide Perovskite Nanocrystals. One of the most striking features of LHPs is their high tolerance toward defects. The term "defect tolerance" here means that, though the optical and electronic properties of perovskites often appear as though there are no electronic traps or excessive doping present, structural and other characterization methods do point to a large density of various structural defects. From the electronic point of view, such behavior suggests preservation of a clean bandgap upon creation of typical defects such as vacancies or surface-related sites because their defect energy levels reside entirely within either the valence band (VB) or the conduction band (CB) manifolds but not within the bandgap itself. In this regard, perovskite NCs are highly unusual;[88] they are highly luminescent without recourse to any electronic surface passivation, whereas such passivation is mandatory to achieve a high PL QY from conventional QDs derived from metal chalcogenides (i.e., CdSe) or metal pnictides (i.e., InP).

Perovskite nanocrystals exhibit high "defect tolerance", meaning that, unlike conventional semiconductors, they can be bright emitters without electronic passivation of their surfaces.

The defect tolerance had been rationalized theoretically for a variety of perovskite compounds. For $CsPbBr_3$, for instance, the surfaces of NCs, point defects in the bulk material,[89] as well as grain boundaries[90] were all shown to either form shallow trap states or to be resonant with VB and CB states. The defect tolerance is partly attributed to the high ionicity of bonding in LHPs. Furthermore, mixing of a Pb lone pair s orbital and an

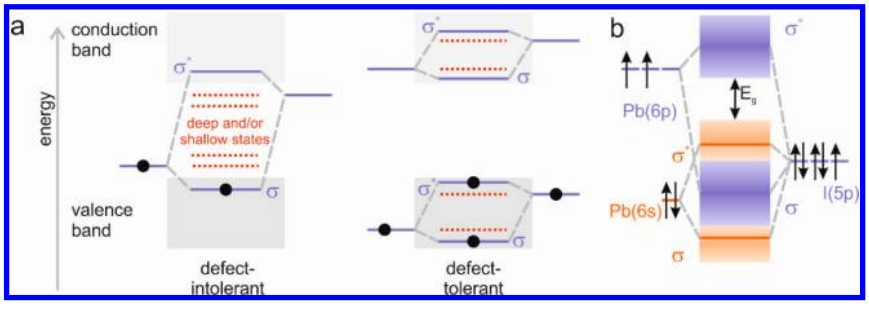

Figure 4. (a) Schematics of two limiting cases of a band-structure in semiconductors: defect-intolerant (conventional, left) and ideal hypothetical defect-tolerant (right). Bonding and antibonding orbitals are denoted as σ and σ^*, respectively. (b) Simplified depiction of the bonding in $APbI_3$ (adapted from ref 96). The VB exhibits the desired antibonding character at its maximum, as in the ideal defect-tolerant case in (a). Copyright 2015, Materials Research Society.

DOI: 10.1021/acsenergylett.7b00547
ACS Energy Lett. 2017, 2, 2071−2083

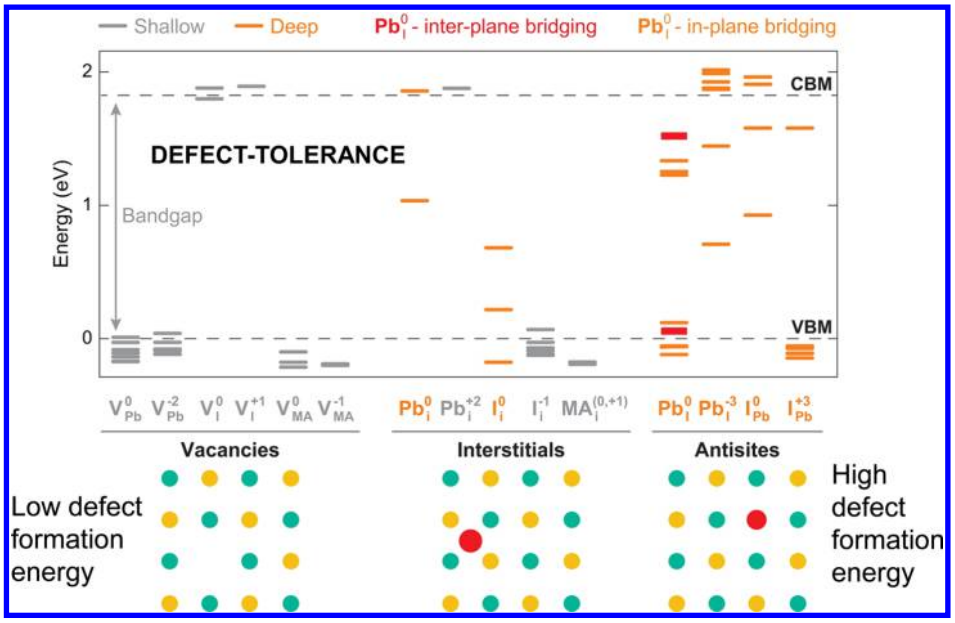

Figure 5. Energy levels associated with the defect states corresponding to neutral and charged vacancies (V_{Pb}, V_I, V_{MA}), neutral and charged interstitials (Pb_i, I_i, MA_i), and neutral and charged states associated with antisites (Pb_I and I_{Pb}) in $MAPbI_3$. Adapted from ref 91. Copyright 2015, American Chemical Society.

iodine p orbital results in antibonding coupling in the perovskite lattice, with the bandgap opening up between two antibonding bands. Because of this band structure, structural defects that may arise from the halide and MA or other A^+-type vacancies tend to have energy levels that fall within the CB and VB, respectively, rather than lying within the bandgap itself. On the contrary, in conventional, defect-intolerant semiconductors such as Si, CdSe, or GaAs, the bandgap is formed between bonding and antibonding orbitals, leading to enclosure of all defect states either as shallow or as midgap states as bonding is locally weakened at all defect sites (point defects, dislocations, planar defects, surfaces, etc.). The comparison is schematically depicted in Figure 4.

A second reason for having clean bandgaps relates to the energy of defect formation in LHPs. Halide and A-site vacancies (V_X and V_A) are easily formed as a pair of Schottky vacancies, thus maintaining overall charge neutrality of the lattice. Fortunately, in the LHPs, other point defects, such as interstitially or antisite misplaced atoms, have much higher energies of formation,[91] often even above the formation energy of the parent compound. This scenario is illustrated in Figure 5 for $MAPbI_3$. On the basis of thermodynamic calculations, ionic compensation of point defects in $MAPbI_3$ has been suggested as a charge carrier concentration self-compensation mechanism.[92] Defect tolerance is similarly expected to be of high relevance also in 2D perovskites.[93] NCs can be robust light emitters, even when a large number of ligands are displaced from the surface, and yet the influence of consequent surface defects in trapping charge carriers is negligible.[94,95]

Synthetic Strategies toward Improving the Stability of Lead Halide Perovskite Nanocrystals. Employing different ligands to improve or change the properties of as-prepared materials is a very common strategy in the colloidal QD field, and this is particularly relevant to increasing the stability of LHP NCs given their innate sensitivity to water and other polar solvents. Figure 6a shows an attempt to use different ligands other than the commonly used OA or OLA by Luo et al.[97] By using branched capping ligands, (3-aminopropyl) triethoxysilane (APTES) and polyhedral oligomeric silsesquioxane (POSS) PSS-[3-(2-aminoethyl)amino]propylheptaisobutyl substituted (NH_2-POSS), the authors showed that APTES and POSS could be used as passivators and stabilizers of $MAPbBr_3$ NCs. PL monitoring under exposure to ethanol under UV lamp irradiation indicated enhanced stability when using those two ligands. Galian and Pérez-Prieto et al. reported $MAPbBr_3$ perovskite NCs with a PL QY of ∼100% by using 2-adamantylammonium bromide (ADBr) as the only capping ligand.[44] The photodarkening of these nanoparticles under prolonged irradiation, attributed to moisture, can be avoided by the formation of cucurbit[7]-uril-adamantyl ammonium host–guest complexes (AD@CB) on the NC surface. Figure 6b demonstrates the higher photostability of $MAPbBr_3$ NCs with the latter coating in toluene dispersions even under water with UV photoirradiation.

Besides the issue of stability in contact with moisture and under irradiation with light, it is well-known that $CsPbI_3$ NCs suffer from a facile cubic perovskite to orthorhombic phase transformation (as demonstrated in Figure 6c(i,ii)), which may be a limiting factor for their optoelectronic applications. By replacing the conventionally used OA with an alkyl phosphinic acid, Wang et al. obtained phase-stable cubic perovskite $CsPbI_3$ NCs (Figure 6c(iii,iv)).[98] By changing the ligands, the as-prepared sample remained luminescent for over 20 days while the OA comparison sample showed no emission to the naked eye.

Producing core–shell structures to increase stability is yet another widely used strategy in colloidal semiconductor QDs. Similar treatments have also been used in perovskite syntheses. Bhaumik et al.[99] reported a putative mixed MA–octylammonium lead bromide perovskite core–shell-type structure (Figure 6d). With a thin shell and little to contrast for the core from the shell in TEM images, it was difficult for the authors to show direct evidence of the formation of a shell; however, indirect evidence from elemental analyses and improved PL stability was taken as tentative evidence of successful shell formation. The emission color was tunable in

DOI: 10.1021/acsenergylett.7b00547
ACS Energy Lett. 2017, 2, 2071−2083

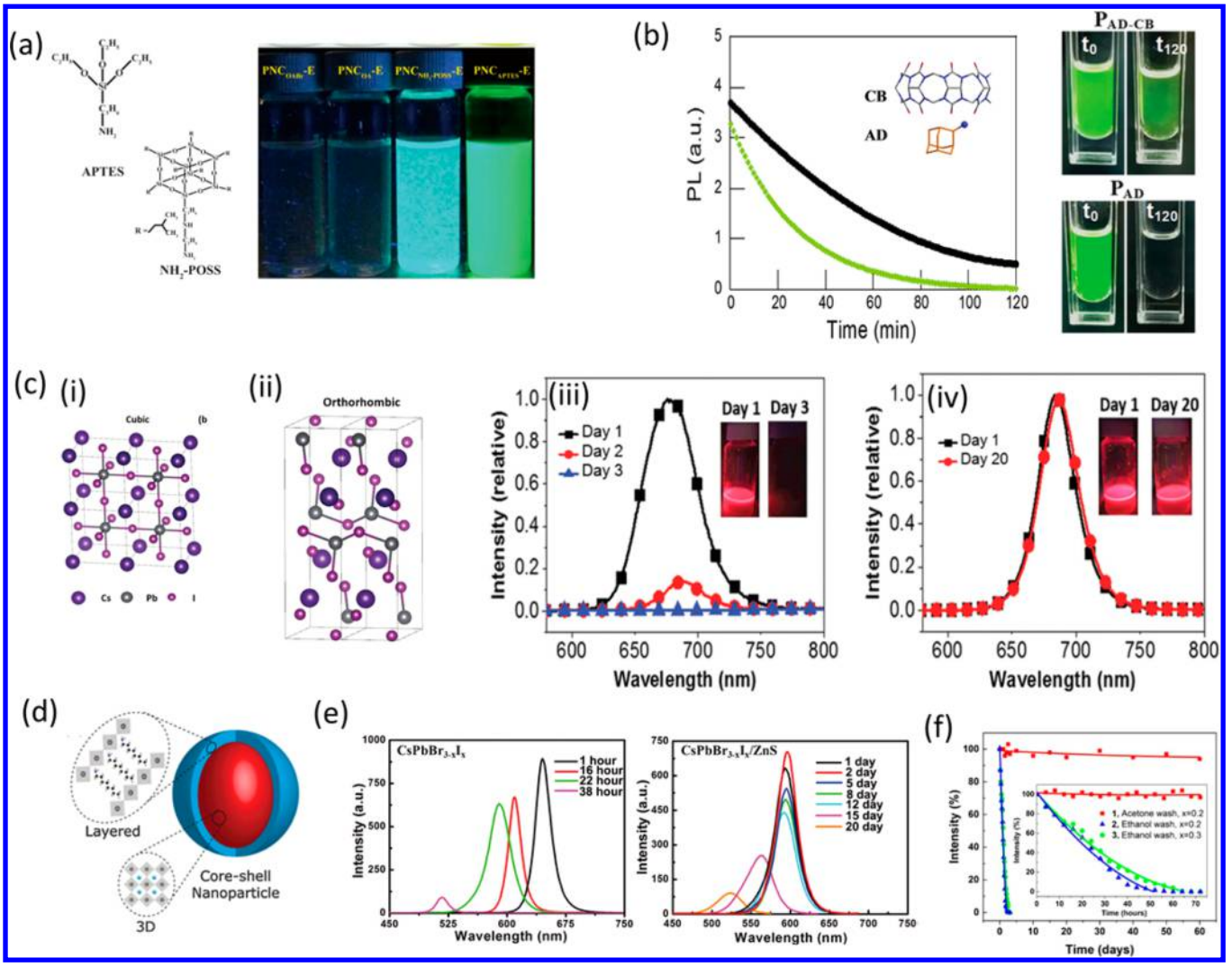

Figure 6. (a) Molecular structure of APTES and NH_2-POSS and photograph of $MAPbBr_3$ NCs (different capping ligands) dispersed in ethanol under UV light. Adapted from ref 97. (b) PL of $MAPbBr_3$ NCs P_{AD-CB} (in black) and P_{AD} (in green) dispersed in toluene and in contact with water as a function of the irradiation time. (Right side) Images of colloidal dispersions immediately after addition (left) of water and 120 min afterward (right); the inset shows the molecular structures of cucurbit[7]uril (CB) and 2-adamantylammonium (AD) ligands. Adapted from ref 44. Copyright 2016 and 2016, Wiley Online Library. (c) Crystal structures of the $CsPbI_3$ (i) cubic and (ii) orthorhombic perovskite. PL spectra for $CsPbI_3$−OA (iii) and $CsPbI_3$−TMPPA (iv). Insets of (iii and iv): Solutions of the respective washed NCs under UV light at different times following synthesis. Adapted from ref 98. (d) Schematics showing the core−shell type of octylammonium lead bromide nanomaterials over $MAPbBr_3$ NPs. Adapted from ref 99. Copyright 2016 and 2016, The Royal Society of Chemistry. (e) Optical stability of $CsPbBr_{3-x}I_x$ and $CsPbBr_{3-x}I_x$/ZnS. Adapted from ref 100. Copyright 2017, Wiley Online Library. (f) PL intensity as a function of time after storing the self-passivation layer formation on mixed-halide perovskite NCs after acetone etching $CsPb(Br_xI_{1-x})_3$ NCs in cyclohexane under ambient conditions. Adapted from ref 101. Copyright 2017, The Royal Society of Chemistry.

the blue to green range by using different MA−octylammonium ratios (438−521 nm), while the PL QY was as high as 92%. Their solution-processed material was reported to be stable at least for 2 months under ambient conditions.

Chen et al. reported a NC architecture made of $CsPbX_3$/ZnS heterodimers synthesized via a facile solution-phase process (Figure 6e).[100] Figure 6e compares the PL stabilities for pure $CsPbBr_{3-x}I_x$ and $CsPbBr_{3-x}I_x$/ZnS heterodimers. The $CsPbBr_{3-x}I_x$ /ZnS heterodimer could keep for about 12 days without any protection in air, while pure $CsPbBr_{3-x}I_x$ QDs became unstable and blue-shifted within 1 day under the same conditions.

Jing et al. found that the stability of mixed-halide $CsPb(Br_xI_{1-x})_3$ NCs could be dramatically enhanced by using a selective acetone etching method.[101] This formed a passivation layer on iodine-rich perovskite NCs by partial iodine etching to instead leave a bromine-rich surface passivation layer (Figure 6f). After the treatment, the PL 50% decay constant was around 17500 h compared with 20 h for the untreated NCs. In other words, the PL stability was increased almost 1000-fold.

In terms of postsynthetic treatments, the employment of silica or silicone derivative coatings on LHP NCs has been proven useful. Huang et al. fabricated SiO_2-encapsulated $MAPbBr_3$ QDs by using a small amount of water in analytical-grade toluene to hydrolyze tetramethyl orthosilicate.[102] Photostability tests were carried out at a relative humidity of 60%, and after 7 h, the PL of the encapsulated powders remained at 94% of the initial value, higher than that

DOI: 10.1021/acsenergylett.7b00547
ACS Energy Lett. 2017, 2, 2071−2083

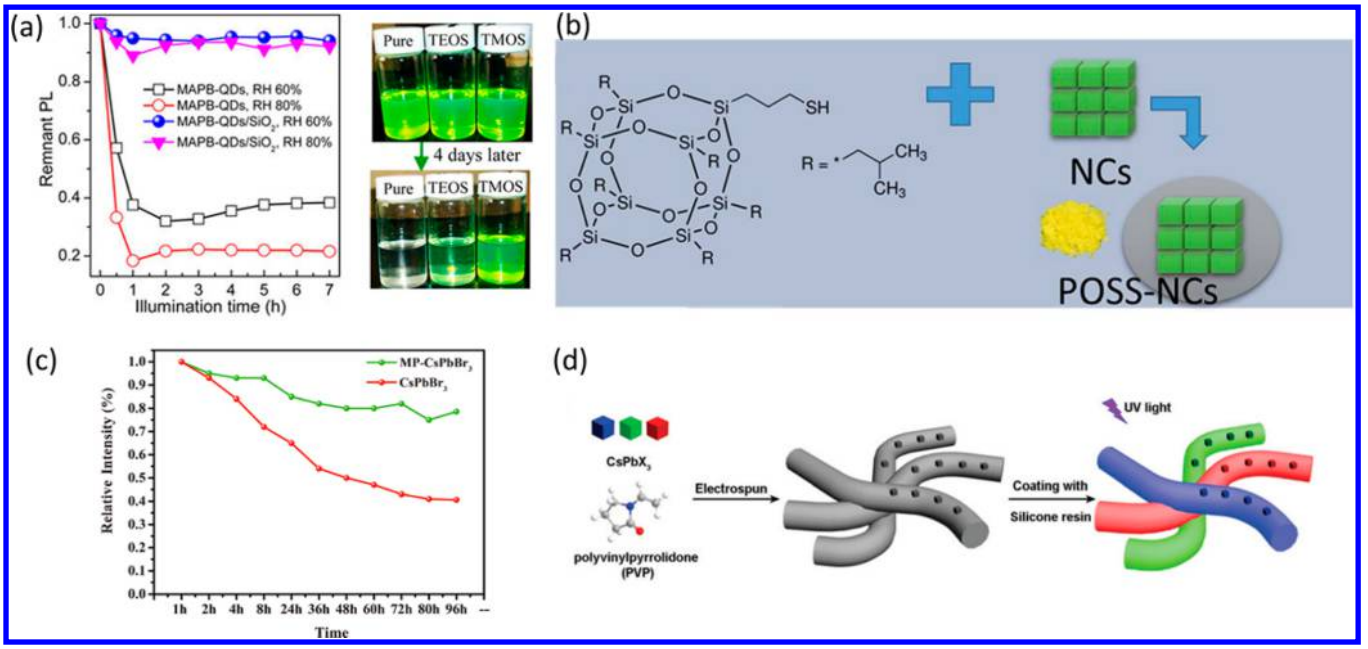

Figure 7. (a) Evaluation of photostability of $MAPbBr_3$(MAPB)-QD and MAPB-QDs/SiO_2 powders in relative humidities (RHs) of 60 and 80% under 470 nm LED light irradiation. Optical images of the as-prepared colloidal MAPB-QD solutions with TEOS and TMOS and storage after 4 days. Adapted from ref 102. Copyright 2016, American Chemical Society. (b) Thiol-functionalized POSS structure: a schematic diagram illustrating the POSS coating process to obtain perovskite NC powders. Adapted from ref 103. Copyright 2016, The Royal Society of Chemistry. (c) Photostability test of MP-$CsPbBr_3$ and $CsPbBr_3$. Adapted from ref 104. Copyright 2016, Wiley Online Library. (d) Schematic of the silicone resin (SR) coating process for the preparation of SR/PVP-$CsPbX_3$. Thermal stability test of SR/PVP-$CsPbBr_3$ and $CsPbBr_3$ QDs. Photostability test of SR/PVP-$CsPbBr_3$ and $CsPbBr_3$ QDs under continuous UV light irradiation. Adapted from ref 105. Copyright 2017, The Royal Society of Chemistry.

for the unencapsulated sample, where the PL had declined to 38% of the original level (Figure 7a).

The first successful water-resistant coating of solid-state perovskite powders was demonstrated by Huang et al.[103] through surface passivation of $CsPbX_3$ (X = Br or I) with POSS molecules, as shown in Figure 7b. In the form of aqueous suspensions, $CsPbX_3$/POSS composites retained their emission unchanged for several months. The POSS coating was also useful when two-color emitters were formed by mixing different composition perovskite NCs as it prevented undesirable anion exchange reactions between the different constituents from occurring in the powder state. The benefits of this passivation strategy were demonstrated when green-emitting POSS-$CsPbBr_3$ and red-emitting POSS-$CsPb(Br/I)_3$ NC powder mixtures were used to fabricate all-perovskite solid-state luminophore down-conversion white light LEDs.

Wang et al. used commercially available mesoporous silica mixed with green $CsPbBr_3$ NCs[104] to similarly bestow water resistance and prevent ion exchange in their mixtures of different composition. The photostability comparison is shown in Figure 7c. By infiltrating perovskite precursors into mesoporous silica after drying, Dirin et al. showed the formation of perovskite NCs entrapped within the pores.[88] Sun et al. used a similar hydrolysis approach[102] with another silica source APTES.[106]

Hai et al. reported a simple fabrication method for emissive flexible films composed of polyvinylpyrrolidone (PVP) as a matrix polymer and codoping blue, green, and red $CsPbX_3$ (X = I, Br, and Cl) as guest fluorophores at various ratios.[105] A schematic of their hydrophobic silicone resin (SR)/PVP NC composite film, SR/PVP-$CsPbX_3$, is presented in Figure 7d. PVP-coated NCs (as single or multiple component mixtures) were electrospun to form nanofiber films using single- or multinozzle electrospinning. To provide further protection from humidity and facilitate handling, SR was deposited onto the surface of the composite electrospun nanofibers to obtain water-stable nanofibrous membranes.

Apart from silica coating, polymer coating has also proved useful in LHP NC passivation. Meyns et al. demonstrated the addition of poly(maleicanhydride-*alt*-1-octadecene) (PMA) into the precursor mixture during the synthesis of perovskite NCs.[107] The normalized integrals of the emission peaks between 460 and 600 nm over 12 h of constant irradiation showed higher emission signals for samples with PMA compared with untreated NCs (Figure 8a). By reducing the ligand surface exchange rate, the ligand binding was tightened in the presence of the PMA, reducing the scope for the NC surface to interact with the surrounding medium, thereby improving the NC stability.

Zhang et al. formed water-resistant polystyrene microhemispheres (MHSs) embedded with $CsPbX_3$ (X = Cl, Br, I) NCs (denoted as NCs@MHSs) as hybrid multicolor and multiplexed optical coding agents.[110] PVP acted as the capping ligand and was adsorbed onto the perovskite NC surface and in doing so formed a protective layer. The PVP surface thus formed also served as an interface layer for further addition of an additional polystyrene matrix allowing the $CsPbX_3$ NCs to be embedded in polymer MHSs. The well-passivated $CsPbX_3$ NCs@MHSs were incorporated into live cells showing high stability and noncytotoxicity and functioned as useful multicolor luminescent probes.

Hou et al. demonstrated stable core−shell colloidal LHP NCs using a copolymer templated synthesis approach.[108] The block copolymer served as a confined nanoreactor during

DOI: 10.1021/acsenergylett.7b00547
ACS Energy Lett. 2017, 2, 2071−2083

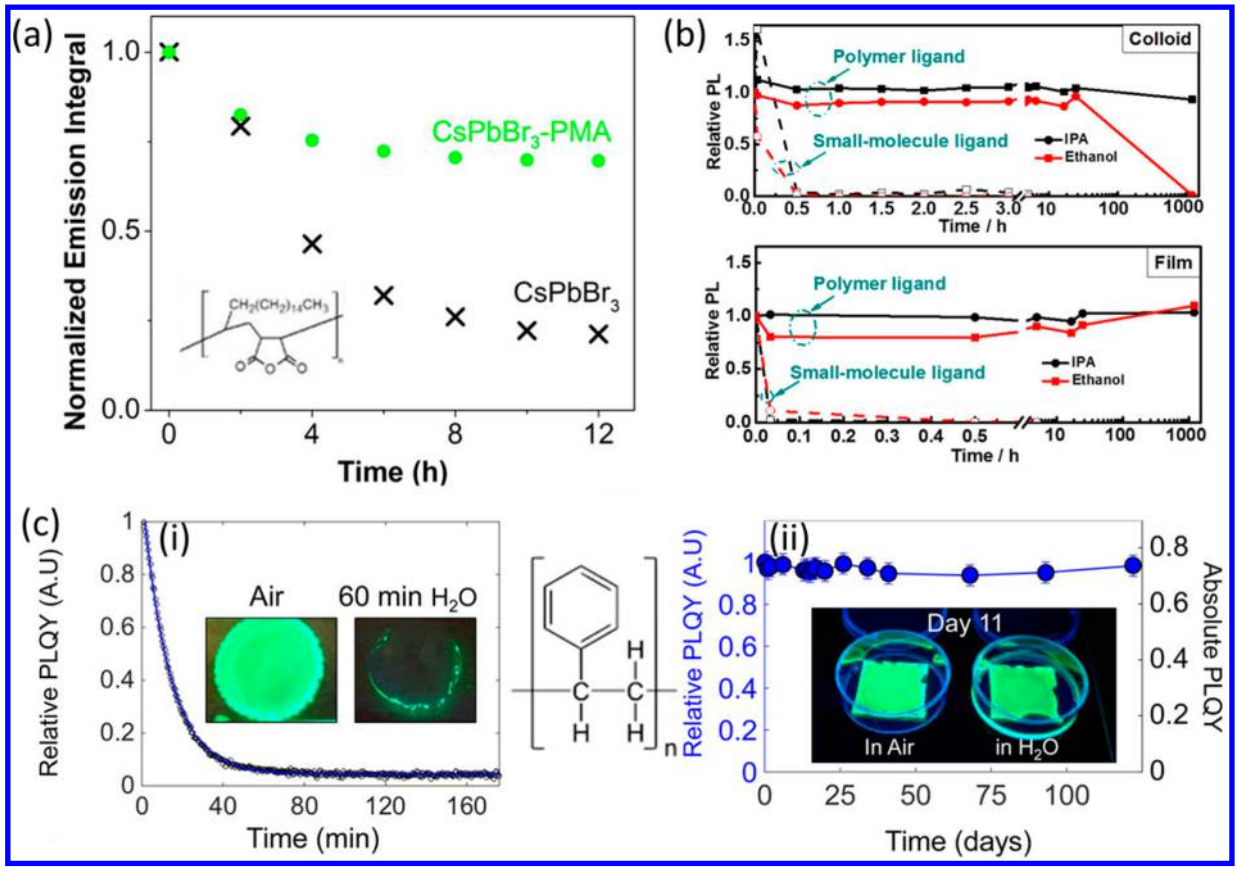

Figure 8. (a) Normalized integrals of the emission peaks between 460 and 600 nm of $CsPbBr_3$ with/without PMA over 12 h of constant irradiation. The inset shows the structure of PMA. Adapted from ref 107. (b) Stability of $CsPbBr_3$ perovskite colloid and film. Perovskite colloids mixed with different solvents (ethanol, IPA). Time evolution of fluorescence intensity after adding 1:1 v:v solvents into perovskite colloids. Time evolution of fluorescence intensity after immersing perovskite/polymer hybrid films in different solvents. Adapted from ref 108. (c) (i) Relative PL QYs of as-synthesized $CsPbBr_3$ NCs in water after different times. Inset pictures show as-synthesized samples before and after 60 min of water soaking under a UV lamp. (ii) Relative and absolute PL QYs of 150 μm thick nanocube polymer composite films after over 4 months of water-soaking. Thin 3 μm composite films also showed enhanced water stability (see inset pictures). Adapted from ref 109. Copyright 2016, 2017, and 2016, respectively, American Chemical Society.

perovskite crystallization and passivated the perovskite surface by forming a multidentate capping shell. The polymer nanoshell provided an additional layer for further surface modifications, useful for self-assembly and so forth and also served to passivate and improve the photostability of the NCs. Figure 8b compares the PL stability of $CsPbBr_3$ NCs with the multidentate copolymer ligand and with small-molecule ligands (OA and OLA) upon exposure to ethanol and propan-2-ol. While OA/OLA-capped NCs quenched immediately after mixing the colloids with both solvents and the PL totally disappeared within 3 h, the multidentate polymer/perovskite NC samples exhibited stable fluorescence after more than 25 h in ethanol and for up to 50 days after adding IPA.

Raja et al. reported enhanced water and light stability by encapsulation of $CsPbBr_3$ NCs into matched presynthesized hydrophobic macroscale polymeric matrixes.[109] Their $CsPbBr_3$ QDs lost all emission after 60 min of contact with water (Figure 8c(i)), while the NC/polymer composite films functioned even after more than 4 months of continuous immersion in water (Figure 8c(ii)). The author also claimed no detectable lead leaching into the water that was in contact with the encapsulated perovskites.

Summary and Future Outlook. There are a number of research avenues related to LHP NCs that will require attention in the forthcoming years. One of the puzzling questions concerns the origin of the significantly blue-shifted PL from $CsPbBr_3$ NCs. Interestingly, both the PL peak and absorption edge from $CsPbBr_3$ NCs never exceed 520 nm, even at NC sizes far beyond the quantum-confinement regime (>20 nm). In fact, bulk $CsPbBr_3$ has an optical band gap at 2.25 eV (551 nm), both in our experiments and in the literature.[111] Our experience shows that the PL peak for NCs larger than 11 nm is always at exactly 520 nm, fully ruling out the quantum size effects at these large sizes as the origin of the blue shift. At present, the atomistic origin of this effect remains unclear. Rather broad X-ray diffraction reflections of $CsPbBr_3$ NCs make it difficult to differentiate between the orthorhombic (nearly cubic) lattice of the bulk material and other possible distortions of the ideal cubic lattice. A recent study suggested significant and dynamic structural disorder that involves formation and re-formation of twin planes between orthorhombic perovskite subdomains in $CsPbBr_3$.[112]

It has been not easy to push the emission of LHP NCs toward the red and near-infrared spectral range while maintaining reasonable material stability. An effective strategy to overcome this so-called "red wall" is mixing larger FA^+ and smaller Cs^+ in one lattice, thereby compensating for the poor individual fits of these ions separately. An additional stabilizing factor in this case is provided by the high entropy of mixing.[80] Formation of mixed-cation compositions in iodide-based LHPs

DOI: 10.1021/acsenergylett.7b00547
ACS Energy Lett. 2017, 2, 2071−2083

has become a major strategy in thin-film solar cell research, yielding the highest power conversion efficiencies of up to 22%: FA/MA,[79,113−115] Cs/MA,[116] Cs/FA,[70,77,78,80] Cs/MA/FA,[117] or even Rb/Cs/MA/FA.[81] Recently, this approach has been extended to LHP NCs, namely, for a (Cs/FA)PbI_3.[53] Similarly, other mixed-cation formulations have been investigated as well, including Au−$CsPbBr_3$, $Cs_{1-x}Rb_xPbBr_3$, and so on.[118−120] Further work will establish the synthesis procedures and elucidate structures for corresponding multinary LHP NCs.

Future synthesis efforts should focus on the protective encapsulation of perovskite nanocrystals.

The defect tolerance of LHP NCs offers strong inspiration to search for similar attributes in other related compounds, especially those that do not contain toxic lead or other heavy metals.[6,121] Similar electronic structures and defect-tolerant behavior are to be expected from the main-group metals, which offer both s and p electrons for the formation of the VB and CB. A first example is through the replacement of Pb^{2+} with Bi^{3+}, an ion of similar size. Yet, the resulting compounds of composition $Cs_3M_2X_9$ (M = Sb, Bi) have vastly different crystal structures, dominated by 0D or 2D networks of Bi−X polyhedra, and exhibit no significant PL at ambient conditions.[122] A full structural analogue of 3D perovskites can be constructed by replacing Pb^{2+} with a 1:1 mixture of M^+ and one M^{3+}, forming so-called double perovskites, $A_2M^+M^{3+}X_6$, such as such as $Cs_2BiAgCl_6$ and $Cs_2AgInCl_6$.[123,124] The electronic band structure of thallium halides also shows a strong resemblance to LHPs.[125] Finally, the most obvious strategy—replacement of Pb^{2+} with Sn^{2+} and Ge^{2+}—has thus far failed due to oxidative instability, even with respect to trace quantities of oxygen. Even trace amounts of Sn^{4+} and Ge^{4+} degenerately dope such semiconductors. In this regard, a somewhat surprising finding is the bright and air-stable emission, albeit with broad fwhm in excess of 100 nm, from $(C_4N_2H_{14}Br)_4SnX_6$ (X = Br, I),[126] a compound comprising isolated SnX_6^{4-} octahedra in a land of large organic cations. One can assume that oxidative stability is enabled by these cations that prevent diffusion of oxygen to the Sn^{2+} sites. This observation might open an avenue to other stable hybrid organic−inorganic lead-free perovskites.

Many strategies discussed in this Perspective for perovskite NC stability enhancement would leave the NCs inaccessible in terms of injection of charges, which could be detrimental for a number of optoelectronic applications. They still have a vast possibility of applications such as color-conversion and color-enhancing layers. If the stability of LHP NCs can successfully be improved, with the narrow PL fwhm of just 18−20 nm in the green at 530 nm ($CsPbBr_3$, $FAPbBr_3$ NCs) and 35 at 630 nm ($CsPb(Br/I)_3$) and high PL QYs of up to 95−100%, LHP NCs may become a strong competitor to traditional colloidal QDs for applications in backlit TV displays and in related color-conversion and color-enhancing applications. At present, two principal types of QD emitters in the red and green have been successfully commercialized in LCD TVs: CdSe-based QDs by Sony in 2014 and InP-based QDs by Samsung in 2015 (under the brand name SUHD TV). Perovskite NCs could be used to replace CdSe or InP QDs in those commercialized LCD TVs, potentially exceeding their performance in terms of color saturation and brightness in the longer term. Under the pressure of increasingly stringent legislation for the use of heavy metals in consumer electronics, Cd use is being limited in such applications. Lead, on the other hand, is exempted for several applications, such as in lead-acid batteries, produced globally on the millions of tons scale. For comparison, one TV display of typical 40−60 in. dimension requires only several mg of QDs,[127] summing up to at most several kilograms at substantial TV display market penetration. LHP NCs could offer strong competition with regard to InP-based QDs arising from the inherently much narrower, size-independent emission, being at 530 nm twice as narrow as the equivalent III−V-based NCs (fwhm ≈ 40 at 530 nm for InP-based QDs).

AUTHOR INFORMATION

Corresponding Authors

*E-mail: mvkovalenko@ethz.ch (M.V.K.).
*E-mail: andrey.rogach@cityu.edu.hk (A.L.R.).

ORCID

He Huang: 0000-0002-2052-718X
Stephen V. Kershaw: 0000-0003-0408-4902
Maksym V. Kovalenko: 0000-0002-6396-8938
Andrey L. Rogach: 0000-0002-8263-8141

Notes

The authors declare no competing financial interest.

Biographies

He Huang received his Bachelors degree in environmental engineering from Chang'an University in 2011 and his Masters degree in environmental engineering from Shanghai University (both China) in 2014. He is now completing his Ph.D. in Prof. Rogach's group at the City University of Hong Kong.

Maryna I. Bodnarchuk is an Ambizione Fellow and a scientist at Empa (Swiss Federal Laboratories for Materials Science and Technology). She received her Masters degree in Inorganic Chemistry from Chernivtsi National University (Ukraine, 2003) and Ph.D. in natural sciences from the Johannes Kepler University Linz (Austria, 2009) and worked as a postdoctoral fellow at the University of Chicago (2010−2011) and as the Marie Heim-Vögtlin Fellow at ETH Zurich (2012−2014). Web page: https://www.empa.ch/web/s207/.

Stephen V. Kershaw is a senior research fellow at the City University of Hong Kong. He received his B.Sc. and Ph.D. from Manchester University, U.K. and later joined British Telecom Laboratories and then Corning's U.K. Research Laboratories. From 2002 until 2010, he was the managing director of a quantum dot startup company in the U.K.

Maksym V. Kovalenko is an associate professor of inorganic chemistry at the Swiss Federal Institute of Technology Zurich (ETH Zurich) and affiliated scientist at Empa (Swiss Federal Laboratories for Materials Science and Technology). He received his Masters degree in Inorganic Chemistry from Chernivtsi National University (Ukraine, 2004) and Ph.D. in nanoscience and nanotechnology from Johannes Kepler University Linz (Austria, 2007) and worked as a postdoctoral fellow at the University of Chicago (2008−2011). Web page: www.kovalenkolab.ethz.ch.

Andrey L. Rogach is a Chair Professor of Photonics Materials and the founding director of the Centre for Functional Photonics at the City University of Hong Kong. He received his diploma in chemistry (1991) and Ph.D. in physical chemistry (1995) from the Belarusian State University in Minsk and worked as a staff scientist at the Universities of Hamburg and Munich (Germany) from 1995 to 2009.

DOI: 10.1021/acsenergylett.7b00547
ACS Energy Lett. 2017, 2, 2071−2083

Web page: http://personal.cityu.edu.hk/~arogatch/Prof%20Andrey%20Rogach.htm.

■ ACKNOWLEDGMENTS

This work was supported by the Research Grant Council of Hong Kong S.A.R. (GRF project CityU 11337616), by the European Research Council under the European Union's Seventh Framework Program: Grant Agreement Nr. 306733 (ERC Starting Grant "NANOSOLID"), and by the Swiss National Science Foundation (SNF Ambizione Energy grant, Grant Nr. PZENP2_154287).

■ REFERENCES

(1) Huang, H.; Polavarapu, L.; Sichert, J. A.; Susha, A. S.; Urban, A. S.; Rogach, A. L. Colloidal Lead Halide Perovskite Nanocrystals: Synthesis, Optical Properties and Applications. *NPG Asia Mater.* **2016**, *8*, e328.

(2) Amgar, D.; Aharon, S.; Etgar, L. Inorganic and Hybrid Organo-Metal Perovskite Nanostructures: Synthesis, Properties, and Applications. *Adv. Funct. Mater.* **2016**, *26*, 8576−8593.

(3) Gonzalez-Carrero, S.; Galian, R. E.; Perez-Prieto, J. Organic-Inorganic and All-Inorganic Lead Halide Nanoparticles. *Opt. Express* **2016**, *24*, A285−301.

(4) Li, X.; Cao, F.; Yu, D.; Chen, J.; Sun, Z.; Shen, Y.; Zhu, Y.; Wang, L.; Wei, Y.; Wu, Y.; et al. All Inorganic Halide Perovskites Nanosystem: Synthesis, Structural Features, Optical Properties and Optoelectronic Applications. *Small* **2017**, *13*, 1603996.

(5) González-Carrero, S.; Galian, R. E.; Pérez-Prieto, J. Organometal Halide Perovskites: Bulk Low-Dimension Materials and Nanoparticles. *Part. Part. Syst. Char.* **2015**, *32*, 709−720.

(6) Swarnkar, A.; Ravi, V. K.; Nag, A. Beyond Colloidal Cesium Lead Halide Perovskite Nanocrystals: Analogous Metal Halides and Doping. *ACS Energy Lett.* **2017**, *2*, 1089−1098.

(7) Kojima, A.; Teshima, K.; Shirai, Y.; Miyasaka, T. Organometal Halide Perovskites as Visible-Light Sensitizers for Photovoltaic Cells. *J. Am. Chem. Soc.* **2009**, *131*, 6050−1.

(8) *National Renewable Energy Laboratory Best Research-Cell Efficiencies*. https://www.nrel.gov/pv/assets/images/efficiency-chart.png (accessed Mar 11, 2017).

(9) Wang, N.; Cheng, L.; Ge, R.; Zhang, S.; Miao, Y.; Zou, W.; Yi, C.; Sun, Y.; Cao, Y.; Yang, R.; et al. Perovskite Light-Emitting Diodes Based on Solution-Processed Self-Organized Multiple Quantum Wells. *Nat. Photonics* **2016**, *10*, 699−704.

(10) Zhang, L.; Yang, X.; Jiang, Q.; Wang, P.; Yin, Z.; Zhang, X.; Tan, H.; Yang, Y. M.; Wei, M.; Sutherland, B. R.; et al. Ultra-Bright and Highly Efficient Inorganic Based Perovskite Light-Emitting Diodes. *Nat. Commun.* **2017**, *8*, 15640.

(11) Wells, H. L. Über die Cäsium- und Kalium-Bleihalogenide. *Z. Anorg. Chem.* **1893**, *3*, 195−210.

(12) Moller, C. K. Crystal Structure and Photoconductivity of Caesium Plumbohalides. *Nature* **1958**, *182*, 1436−1436.

(13) Sharma, S.; Weiden, N.; Weiss, A. Phase-Diagrams of Quasi-Binary Systems of the Type - ABX_3-$A'BX_3$ ABX_3-$AB'X_3$, AND ABX_3-ABX'_3 X = Halogen. *Z. Phys. Chem.* **1992**, *175*, 63−80.

(14) Trots, D. M.; Myagkota, S. V. High-Temperature Structural Evolution of Caesium and Rubidium Triiodoplumbates. *J. Phys. Chem. Solids* **2008**, *69*, 2520−2526.

(15) Stoumpos, C. C.; Malliakas, C. D.; Kanatzidis, M. G. Semiconducting Tin and Lead Iodide Perovskites with Organic Cations: Phase Transitions, High Mobilities, and Near-Infrared Photoluminescent Properties. *Inorg. Chem.* **2013**, *52*, 9019−9038.

(16) Babin, V.; Fabeni, P.; Nikl, M.; Nitsch, K.; Pazzi, G. P.; Zazubovich, S. Luminescent $CsPbI_3$ and CS_4PbI_6 Aggregates in Annealed CsI: Pb Crystals. *Phys. Status Solidi B* **2001**, *226*, 419−428.

(17) Sharma, S.; Weiden, N.; Weiss, A. ^{207}Pb and ^{205}Tl NMR on Perovskite Type Crystals $APbX_3$ (A = Cs, Tl, X = Br, I). *Z. Naturforsch., A: Phys. Sci.* **1987**, *42*, 1313−1320.

(18) Sakudo, T.; Unoki, H.; Fujii, Y.; Kobayashi, J.; Yamada, M. A New Structural Phase Transition in $CsPbCl_3$. *Phys. Lett. A* **1969**, *28*, 542−543.

(19) Hirotsu, S.; Sawada, S. Crystal Growth and Phase Transitions of $CsPbCl_3$. *Phys. Lett. A* **1969**, *28*, 762−763.

(20) Tovborg-Jensen, N. NQR Investigation of Phase Transitions in Cesium Plumbochloride. *J. Chem. Phys.* **1969**, *50*, 559−560.

(21) Cape, J. A.; White, R. L.; Feigelson, R. S. EPR Study of the Structure of $CsPbCl_3$. *J. Appl. Phys.* **1969**, *40*, 5001−5005.

(22) Hirotsu, S. Experimental Studies of Structural Phase Transitions in $CsPbCl_3$. *J. Phys. Soc. Jpn.* **1971**, *31*, 552−560.

(23) Fujii, Y.; Hoshino, S.; Yamada, Y.; Shirane, G. Neutron-Scattering Study on Phase Transitions of $CsPbCl_3$. *Phys. Rev. B* **1974**, *9*, 4549−4559.

(24) Armstrong, R. L.; Lourens, J. A. J.; Stroud, J. D. ^{133}Cs Spin-Lattice Relaxation Study of Phase Transitions in $CsPbCl_3$. *Phys. Rev. B* **1976**, *13*, 5099−5101.

(25) Hidaka, M.; Okamoto, Y.; Zikumaru, Y. Structural Phase Transition of $CsPbCl_3$ below Room Temperature. *Phys. Status Solidi A* **1983**, *79*, 263−269.

(26) Moller, C. K. A Phase Transition in Caesium Plumbochloride. *Nature* **1957**, *180*, 981−982.

(27) Armstrong, R. L. Pure Nuclear Quadrupole Resonance Studies of Structural Phase Transitions. *J. Magn. Reson. (1969-1992)* **1975**, *20*, 214−231.

(28) van Driel, H. M.; Armstrong, R. L. ^{35}Cl Spin-Lattice Relaxation Study of Phase Transitions in $CsPbCl_3$. *Phys. Rev. B* **1975**, *12*, 839−841.

(29) Poulsen, F. R.; et al. Crystal Structure and Phase Transition of Cesium Trichlorostannate(II). *Acta Chem. Scand.* **1970**, *24*, 150−156.

(30) Scaife, D. E.; Weller, P. F.; Fisher, W. G. Crystal Preparation and Properties of Cesium Tin(II) Trihalides. *J. Solid State Chem.* **1974**, *9*, 308−314.

(31) Barrett, J.; Bird, S. R. A.; Donaldson, J. D.; Silver, J. The Mössbauer Effect in Tin(II) Compounds. Part XI. The Spectra of Cubic Trihalogenostannates(II). *J. Chem. Soc. A* **1971**, *0*, 3105−3108.

(32) Clark, S. J.; Flint, C. D.; Donaldson, J. D. Luminescence and Electrical Conductivity of $CsSnBr_3$, and Related Phases. *J. Phys. Chem. Solids* **1981**, *42*, 133−135.

(33) Christensen, A. N.; et al. A Ferroeletric Chloride of Perowskite Type. Crystal Structure of $CsGeCl_3$. *Acta Chem. Scand.* **1965**, *19*, 421.

(34) Weber, D. $CH_3NH_3PbX_3$, ein Pb (II)-System mit Kubischer Perowskitstruktur/$CH_3NH_3PbX_3$, a Pb (II)-System with Cubic Perovskite Structure. *Z. Naturforsch. B* **1978**, *33*, 1443−1445.

(35) Protesescu, L.; Yakunin, S.; Bodnarchuk, M. I.; Krieg, F.; Caputo, R.; Hendon, C. H.; Yang, R. X.; Walsh, A.; Kovalenko, M. V. Nanocrystals of Cesium Lead Halide Perovskites ($CsPbX_3$, X = Cl, Br, and I): Novel Optoelectronic Materials Showing Bright Emission with Wide Color Gamut. *Nano Lett.* **2015**, *15*, 3692−3696.

(36) Rogach, A. L. *Semiconductor Nanocrystal Quantum Dots*; Springer Vienna: Vienna, Austria, 2008; pp 1−372.

(37) Goldschmidt, V. M. Die Gesetze der Krystallochemie. *Naturwissenschaften* **1926**, *14*, 477−485.

(38) Saparov, B.; Mitzi, D. B. Organic-Inorganic Perovskites: Structural Versatility for Functional Materials Design. *Chem. Rev.* **2016**, *116*, 4558−4596.

(39) Zhang, F.; Zhong, H.; Chen, C.; Wu, X. G.; Hu, X.; Huang, H.; Han, J.; Zou, B.; Dong, Y. Brightly Luminescent and Color-Tunable Colloidal $CH_3NH_3PbX_3$ (X = Br, I, Cl) Quantum Dots: Potential Alternatives for Display Technology. *ACS Nano* **2015**, *9*, 4533−4542.

(40) Huang, H.; Susha, A. S.; Kershaw, S. V.; Hung, T. F.; Rogach, A. L. Control of Emission Color of High Quantum Yield $CH_3NH_3PbBr_3$ Perovskite Quantum Dots by Precipitation Temperature. *Adv. Sci.* **2015**, *2*, 1500194.

(41) Tong, Y.; Ehrat, F.; Vanderlinden, W.; Cardenas-Daw, C.; Stolarczyk, J. K.; Polavarapu, L.; Urban, A. S. Dilution-Induced Formation of Hybrid Perovskite Nanoplatelets. *ACS Nano* **2016**, *10*, 10936−10944.

DOI: 10.1021/acsenergylett.7b00547
ACS Energy Lett. 2017, 2, 2071−2083

(42) Sichert, J. A.; Tong, Y.; Mutz, N.; Vollmer, M.; Fischer, S.; Milowska, K. Z.; Garcia Cortadella, R.; Nickel, B.; Cardenas-Daw, C.; Stolarczyk, J. K.; et al. Quantum Size Effect in Organometal Halide Perovskite Nanoplatelets. *Nano Lett.* **2015**, *15*, 6521−7.
(43) Schmidt, L. C.; Pertegas, A.; Gonzalez-Carrero, S.; Malinkiewicz, O.; Agouram, S.; Minguez Espallargas, G.; Bolink, H. J.; Galian, R. E.; Perez-Prieto, J. Nontemplate Synthesis of $CH_3NH_3PbBr_3$ Perovskite Nanoparticles. *J. Am. Chem. Soc.* **2014**, *136*, 850−853.
(44) Gonzalez-Carrero, S.; Frances-Soriano, L.; Gonzalez-Bejar, M.; Agouram, S.; Galian, R. E.; Perez-Prieto, J. The Luminescence of $CH_3NH_3PbBr_3$ Perovskite Nanoparticles Crests the Summit and Their Photostability under Wet Conditions is Enhanced. *Small* **2016**, *12*, 5245−5250.
(45) Zhang, F.; Huang, S.; Wang, P.; Chen, X. M.; Zhao, S. L.; Dong, Y. P.; Zhong, H. Z. Colloidal Synthesis of Air-Stable $CH_3NH_3PbI_3$ Quantum Dots by Gaining Chemical Insight into the Solvent Effects. *Chem. Mater.* **2017**, *29*, 3793−3799.
(46) Zhou, Q.; Bai, Z.; Lu, W. G.; Wang, Y.; Zou, B.; Zhong, H. In Situ Fabrication of Halide Perovskite Nanocrystal-Embedded Polymer Composite Films with Enhanced Photoluminescence for Display Backlights. *Adv. Mater.* **2016**, *28*, 9163−9168.
(47) Niu, Y.; Zhang, F.; Bai, Z.; Dong, Y.; Yang, J.; Liu, R.; Zou, B.; Li, J.; Zhong, H. Aggregation-Induced Emission Features of Organometal Halide Perovskites and Their Fluorescence Probe Applications. *Adv. Opt. Mater.* **2015**, *3*, 112−119.
(48) Tyagi, P.; Arveson, S. M.; Tisdale, W. A. Colloidal Organohalide Perovskite Nanoplatelets Exhibiting Quantum Confinement. *J. Phys. Chem. Lett.* **2015**, *6*, 1911−6.
(49) Huang, H.; Xue, Q.; Chen, B.; Xiong, Y.; Schneider, J.; Zhi, C.; Zhong, H.; Rogach, A. L. Top-Down Fabrication of Stable Methylammonium Lead Halide Perovskite Nanocrystals Employing a Mixture of Ligands as Coordinating Solvents. *Angew. Chem., Int. Ed.* **2017**, *56*, 9571−9576.
(50) Hintermayr, V. A.; Richter, A. F.; Ehrat, F.; Doblinger, M.; Vanderlinden, W.; Sichert, J. A.; Tong, Y.; Polavarapu, L.; Feldmann, J.; Urban, A. S. Tuning the Optical Properties of Perovskite Nanoplatelets through Composition and Thickness by Ligand-Assisted Exfoliation. *Adv. Mater.* **2016**, *28*, 9478−9485.
(51) Tong, Y.; Bladt, E.; Ayguler, M. F.; Manzi, A.; Milowska, K. Z.; Hintermayr, V. A.; Docampo, P.; Bals, S.; Urban, A. S.; Polavarapu, L.; et al. Highly Luminescent Cesium Lead Halide Perovskite Nanocrystals with Tunable Composition and Thickness by Ultrasonication. *Angew. Chem., Int. Ed.* **2016**, *55*, 13887−13892.
(52) Rogach, A. L.; Eychmuller, A.; Hickey, S. G.; Kershaw, S. V. Infrared-Emitting Colloidal Nanocrystals: Synthesis, Assembly, Spectroscopy, and Applications. *Small* **2007**, *3*, 536−557.
(53) Protesescu, L.; Yakunin, S.; Kumar, S.; Bar, J.; Bertolotti, F.; Masciocchi, N.; Guagliardi, A.; Grotevent, M.; Shorubalko, I.; Bodnarchuk, M. I.; et al. Dismantling the "Red Wall" of Colloidal Perovskites: Highly Luminescent Formamidinium and Formamidinium-Cesium Lead Iodide Nanocrystals. *ACS Nano* **2017**, *11*, 3119−3134.
(54) Juarez-Perez, E. J.; Hawash, Z.; Raga, S. R.; Ono, L. K.; Qi, Y. Thermal Degradation of $CH_3NH_3PbI_3$ Perovskite into NH_3 and CH_3I Gases Observed by Coupled Thermogravimetry−Mass Spectrometry Analysis. *Energy Environ. Sci.* **2016**, *9*, 3406−3410.
(55) Conings, B.; Drijkoningen, J.; Gauquelin, N.; Babayigit, A.; D'Haen, J.; D'Olieslaeger, L.; Ethirajan, A.; Verbeeck, J.; Manca, J.; Mosconi, E.; et al. Intrinsic Thermal Instability of Methylammonium Lead Trihalide Perovskite. *Adv. Energy Mater.* **2015**, *5*, 1500477.
(56) De Roo, J.; Ibanez, M.; Geiregat, P.; Nedelcu, G.; Walravens, W.; Maes, J.; Martins, J. C.; Van Driessche, I.; Kovalenko, M. V.; Hens, Z. Highly Dynamic Ligand Binding and Light Absorption Coefficient of Cesium Lead Bromide Perovskite Nanocrystals. *ACS Nano* **2016**, *10*, 2071−2081.
(57) Pan, J.; Sarmah, S. P.; Murali, B.; Dursun, I.; Peng, W.; Parida, M. R.; Liu, J.; Sinatra, L.; Alyami, N.; Zhao, C.; et al. Air-Stable Surface-Passivated Perovskite Quantum Dots for Ultra-Robust, Single- and Two-Photon-Induced Amplified Spontaneous Emission. *J. Phys. Chem. Lett.* **2015**, *6*, 5027−5033.
(58) Yassitepe, E.; Yang, Z.; Voznyy, O.; Kim, Y.; Walters, G.; Castañeda, J. A.; Kanjanaboos, P.; Yuan, M.; Gong, X.; Fan, F.; et al. Amine-Free Synthesis of Cesium Lead Halide Perovskite Quantum Dots for Efficient Light-Emitting Diodes. *Adv. Funct. Mater.* **2016**, *26*, 8757−8763.
(59) Loiudice, A.; Saris, S.; Oveisi, E.; Alexander, D. T. L.; Buonsanti, R. $CsPbBr_3$ QD/AlO_x Inorganic Nanocomposites with Exceptional Stability in Water, Light and Heat. *Angew. Chem., Int. Ed.* **2017**, DOI: 10.1002/anie.201703703.
(60) Li, Z.; Kong, L.; Huang, S.; Li, L. Highly Luminescent and Ultra-Stable $CsPbBr_3$ Pervoskite Quantum Dots-silica/alumina Monolith. *Angew. Chem., Int. Ed.* **2017**, *56*, 8134−8138.
(61) Han, Q.; Bae, S. H.; Sun, P.; Hsieh, Y. T.; Yang, Y. M.; Rim, Y. S.; Zhao, H.; Chen, Q.; Shi, W.; Li, G.; et al. Single Crystal Formamidinium Lead Iodide ($FAPbI_3$): Insight into the Structural, Optical, and Electrical Properties. *Adv. Mater.* **2016**, *28*, 2253−2258.
(62) Saidaminov, M. I.; Abdelhady, A. L.; Murali, B.; Alarousu, E.; Burlakov, V. M.; Peng, W.; Dursun, I.; Wang, L.; He, Y.; Maculan, G.; et al. High-Quality Bulk Hybrid Perovskite Single Crystals within Minutes by Inverse Temperature Crystallization. *Nat. Commun.* **2015**, *6*, 7586.
(63) Saidaminov, M. I.; Abdelhady, A. L.; Maculan, G.; Bakr, O. M. Retrograde Solubility of Formamidinium and Methylammonium Lead Halide Perovskites Enabling Rapid Single Crystal Growth. *Chem. Commun.* **2015**, *51*, 17658−17661.
(64) Liu, Y.; Sun, J.; Yang, Z.; Yang, D.; Ren, X.; Xu, H.; Yang, Z.; Liu, S. F. 20-mm-Large Single-Crystalline Formamidinium-Perovskite Wafer for Mass Production of Integrated Photodetectors. *Adv. Opt. Mater.* **2016**, *4*, 1829−1837.
(65) Zhumekenov, A. A.; Saidaminov, M. I.; Haque, M. A.; Alarousu, E.; Sarmah, S. P.; Murali, B.; Dursun, I.; Miao, X.-H.; Abdelhady, A. L.; Wu, T.; et al. Formamidinium Lead Halide Perovskite Crystals with Unprecedented Long Carrier Dynamics and Diffusion Length. *ACS Energy Lett.* **2016**, *1*, 32−37.
(66) Fang, H.-H.; Wang, F.; Adjokatse, S.; Zhao, N.; Loi, M. A. Photoluminescence Enhancement in Formamidinium Lead Iodide Thin Films. *Adv. Funct. Mater.* **2016**, *26*, 4653−4659.
(67) Palazon, F.; Akkerman, Q. A.; Prato, M.; Manna, L. X-ray Lithography on Perovskite Nanocrystals Films: From Patterning with Anion-Exchange Reactions to Enhanced Stability in Air and Water. *ACS Nano* **2016**, *10*, 1224−1230.
(68) Ma, F.; Li, J.; Li, W.; Lin, N.; Wang, L.; Qiao, J. Stable Alpha/Delta Phase Junction of Formamidinium Lead Iodide Perovskites for Enhanced Near-Infrared Emission. *Chem. Sci.* **2017**, *8*, 800−805.
(69) Eperon, G. E.; Paternò, G. M.; Sutton, R. J.; Zampetti, A.; Haghighirad, A. A.; Cacialli, F.; Snaith, H. J. Inorganic Caesium Lead Iodide Perovskite Solar Cells. *J. Mater. Chem. A* **2015**, *3*, 19688−19695.
(70) Li, Z.; Yang, M.; Park, J.-S.; Wei, S.-H.; Berry, J. J.; Zhu, K. Stabilizing Perovskite Structures by Tuning Tolerance Factor: Formation of Formamidinium and Cesium Lead Iodide Solid-State Alloys. *Chem. Mater.* **2016**, *28*, 284−292.
(71) Travis, W.; Glover, E. N. K.; Bronstein, H.; Scanlon, D. O.; Palgrave, R. G. On the Application of the Tolerance Factor to Inorganic and Hybrid Halide Perovskites: a Revised System. *Chem. Sci.* **2016**, *7*, 4548−4556.
(72) Kieslich, G.; Sun, S.; Cheetham, A. K. An Extended Tolerance Factor Approach for Organic−Inorganic Perovskites. *Chem. Sci.* **2015**, *6*, 3430−3433.
(73) Kieslich, G.; Sun, S.; Cheetham, A. K. Solid-State Principles Applied to Organic−Inorganic Perovskites: New Tricks for an Old Dog. *Chem. Sci.* **2014**, *5*, 4712−4715.
(74) Filip, M. R.; Eperon, G. E.; Snaith, H. J.; Giustino, F. Steric Engineering of Metal-Halide Perovskites with Tunable Optical Band Gaps. *Nat. Commun.* **2014**, *5*, 5757.
(75) Nazarenko, O.; Yakunin, S.; Morad, V.; Cherniukh, I.; Kovalenko, M. V. Single Crystals of Caesium Formamidinium Lead

DOI: 10.1021/acsenergylett.7b00547
ACS Energy Lett. 2017, 2, 2071−2083

Halide Perovskites: Solution Growth and Gamma Dosimetry. *NPG Asia Mater.* **2017**, *9*, e373.
(76) Chen, D.; Chen, X.; Wan, Z.; Fang, G. Full-Spectral Fine-Tuning Visible Emissions from Cation Hybrid $Cs_{1-m}FA_mPbX3$ (X = Cl, Br, and I, 0 < /= m < /= 1) Quantum Dots. *ACS Appl. Mater. Interfaces* **2017**, *9*, 20671−20678.
(77) Lee, J.-W.; Kim, D.-H.; Kim, H.-S.; Seo, S.-W.; Cho, S. M.; Park, N.-G. Formamidinium and Cesium Hybridization for Photo- and Moisture-Stable Perovskite Solar Cell. *Adv. Energy Mater.* **2015**, *5*, 1501310.
(78) McMeekin, D. P.; Sadoughi, G.; Rehman, W.; Eperon, G. E.; Saliba, M.; Horantner, M. T.; Haghighirad, A.; Sakai, N.; Korte, L.; Rech, B.; et al. A Mixed-Cation Lead Mixed-Halide Perovskite Absorber for Tandem Solar Cells. *Science* **2016**, *351*, 151−155.
(79) Jeon, N. J.; Noh, J. H.; Yang, W. S.; Kim, Y. C.; Ryu, S.; Seo, J.; Seok, S. I. Compositional Engineering of Perovskite Materials for High-Performance Solar Cells. *Nature* **2015**, *517*, 476−480.
(80) Yi, C.; Luo, J.; Meloni, S.; Boziki, A.; Ashari-Astani, N.; Grätzel, C.; Zakeeruddin, S. M.; Röthlisberger, U.; Grätzel, M. Entropic Stabilization of Mixed A-Cation ABX_3 Metal Halide Perovskites for High Performance Perovskite Solar Cells. *Energy Environ. Sci.* **2016**, *9*, 656−662.
(81) Saliba, M.; Matsui, T.; Domanski, K.; Seo, J. Y.; Ummadisingu, A.; Zakeeruddin, S. M.; Correa-Baena, J. P.; Tress, W. R.; Abate, A.; Hagfeldt, A.; et al. Incorporation of Rubidium Cations into Perovskite Solar Cells Improves Photovoltaic Performance. *Science* **2016**, *354*, 206−209.
(82) Gupta, S.; Kershaw, S. V.; Rogach, A. L. 25th Anniversary Article: Ion Exchange in Colloidal Nanocrystals. *Adv. Mater.* **2013**, *25*, 6923−43.
(83) Saruyama, M.; So, Y. G.; Kimoto, K.; Taguchi, S.; Kanemitsu, Y.; Teranishi, T. Spontaneous Formation of Wurzite-CdS/Zinc Blende-CdTe Heterodimers through a Partial Anion Exchange Reaction. *J. Am. Chem. Soc.* **2011**, *133*, 17598−601.
(84) Dawood, F.; Schaak, R. E. ZnO-Templated Synthesis of Wurtzite-Type ZnS and ZnSe Nanoparticles. *J. Am. Chem. Soc.* **2009**, *131*, 424−5.
(85) Erdem, T.; Demir, H. V. Color science of nanocrystal quantum dots for lighting and displays. *Nanophotonics* **2013**, *2*, 57−81.
(86) Raino, G.; Nedelcu, G.; Protesescu, L.; Bodnarchuk, M. I.; Kovalenko, M. V.; Mahrt, R. F.; Stoferle, T. Single Cesium Lead Halide Perovskite Nanocrystals at Low Temperature: Fast Single-Photon Emission, Reduced Blinking, and Exciton Fine Structure. *ACS Nano* **2016**, *10*, 2485−2490.
(87) Swarnkar, A.; Chulliyil, R.; Ravi, V. K.; Irfanullah, M.; Chowdhury, A.; Nag, A. Colloidal $CsPbBr_3$ Perovskite Nanocrystals: Luminescence beyond Traditional Quantum Dots. *Angew. Chem.* **2015**, *127*, 15644−15648.
(88) Dirin, D. N.; Protesescu, L.; Trummer, D.; Kochetygov, I. V.; Yakunin, S.; Krumeich, F.; Stadie, N. P.; Kovalenko, M. V. Harnessing Defect-Tolerance at the Nanoscale: Highly Luminescent Lead Halide Perovskite Nanocrystals in Mesoporous Silica Matrixes. *Nano Lett.* **2016**, *16*, 5866−5874.
(89) Kang, J.; Wang, L. W. High Defect Tolerance in Lead Halide Perovskite $CsPbBr_3$. *J. Phys. Chem. Lett.* **2017**, *8*, 489−493.
(90) Guo, Y.; Wang, Q.; Saidi, W. A. Structural Stabilities and Electronic Properties of High-Angle Grain Boundaries in Perovskite Cesium Lead Halides. *J. Phys. Chem. C* **2017**, *121*, 1715−1722.
(91) Buin, A.; Pietsch, P.; Xu, J.; Voznyy, O.; Ip, A. H.; Comin, R.; Sargent, E. H. Materials Processing Routes to Trap-free Halide Perovskites. *Nano Lett.* **2014**, *14*, 6281−6286.
(92) Walsh, A.; Scanlon, D. O.; Chen, S.; Gong, X. G.; Wei, S. H. Self-Regulation Mechanism for Charged Point Defects in Hybrid Halide Perovskites. *Angew. Chem., Int. Ed.* **2015**, *54*, 1791−1794.
(93) Pandey, M.; Jacobsen, K. W.; Thygesen, K. S. Band Gap Tuning and Defect Tolerance of Atomically Thin Two-Dimensional Organic-Inorganic Halide Perovskites. *J. Phys. Chem. Lett.* **2016**, *7*, 4346−4352.
(94) ten Brinck, S.; Infante, I. Surface Termination, Morphology, and Bright Photoluminescence of Cesium Lead Halide Perovskite Nanocrystals. *ACS Energy Lett.* **2016**, *1*, 1266−1272.
(95) Yettapu, G. R.; Talukdar, D.; Sarkar, S.; Swarnkar, A.; Nag, A.; Ghosh, P.; Mandal, P. Terahertz Conductivity within Colloidal CsPbBr3 Perovskite Nanocrystals: Remarkably High Carrier Mobilities and Large Diffusion Lengths. *Nano Lett.* **2016**, *16*, 4838−48.
(96) Brandt, R. E.; Stevanović, V.; Ginley, D. S.; Buonassisi, T. Identifying Defect-Tolerant Semiconductors with High Minority-Carrier Lifetimes: Beyond Hybrid Lead Halide Perovskites. *MRS Commun.* **2015**, *5*, 265−275.
(97) Luo, B.; Pu, Y. C.; Lindley, S. A.; Yang, Y.; Lu, L.; Li, Y.; Li, X.; Zhang, J. Z. Organolead Halide Perovskite Nanocrystals: Branched Capping Ligands Control Crystal Size and Stability. *Angew. Chem., Int. Ed.* **2016**, *55*, 8864−8868.
(98) Wang, C.; Chesman, A. S.; Jasieniak, J. J. Stabilizing the Cubic Perovskite Phase of $CsPbI_3$ Nanocrystals by Using an Alkyl Phosphinic Acid. *Chem. Commun.* **2017**, *53*, 232−235.
(99) Bhaumik, S.; Veldhuis, S. A.; Ng, Y. F.; Li, M.; Muduli, S. K.; Sum, T. C.; Damodaran, B.; Mhaisalkar, S.; Mathews, N. Highly Stable, Luminescent Core-Shell Type Methylammonium-Octylammonium Lead Bromide Layered Perovskite Nanoparticles. *Chem. Commun.* **2016**, *52*, 7118−7121.
(100) Chen, W.; Hao, J.; Hu, W.; Zang, Z.; Tang, X.; Fang, L.; Niu, T.; Zhou, M. Enhanced Stability and Tunable Photoluminescence in Perovskite $CsPbX_3$ /ZnS Quantum Dot Heterostructure. *Small* **2017**, *13*, 1604085.
(101) Jing, Q.; Zhang, M.; Huang, X.; Ren, X.; Wang, P.; Lu, Z. Surface Passivation of Mixed-Halide Perovskite $CsPb(Br_xI_{1-x})_3$ Nanocrystals by Selective Etching for Improved Stability. *Nanoscale* **2017**, *9*, 7391−7396.
(102) Huang, S.; Li, Z.; Kong, L.; Zhu, N.; Shan, A.; Li, L. Enhancing the Stability of $CH_3NH_3PbBr_3$ Quantum Dots by Embedding in Silica Spheres Derived from Tetramethyl Orthosilicate in "Waterless" Toluene. *J. Am. Chem. Soc.* **2016**, *138*, 5749−5752.
(103) Huang, H.; Chen, B.; Wang, Z.; Hung, T. F.; Susha, A. S.; Zhong, H.; Rogach, A. L. Water Resistant $CsPbX_3$ Nanocrystals Coated with Polyhedral Oligomeric Silsesquioxane and Their Use as Solid State Luminophores in All-Perovskite White Light-Emitting Devices. *Chem. Sci.* **2016**, *7*, 5699−5703.
(104) Wang, H. C.; Lin, S. Y.; Tang, A. C.; Singh, B. P.; Tong, H. C.; Chen, C. Y.; Lee, Y. C.; Tsai, T. L.; Liu, R. S. Mesoporous Silica Particles Integrated with All-Inorganic $CsPbBr_3$ Perovskite Quantum-Dot Nanocomposites (MP-PQDs) with High Stability and Wide Color Gamut Used for Backlight Display. *Angew. Chem., Int. Ed.* **2016**, *55*, 7924−7929.
(105) Hai, J.; Li, H.; Zhao, Y.; Chen, F.; Peng, Y.; Wang, B. Designing of Blue, Green, and Red $CsPbX_3$ Perovskite-Codoped Flexible Films with Water Resistant Property and Elimination of Anion-Exchange for Tunable White Light Emission. *Chem. Commun.* **2017**, *53*, 5400−5403.
(106) Sun, C.; Zhang, Y.; Ruan, C.; Yin, C.; Wang, X.; Wang, Y.; Yu, W. W. Efficient and Stable White LEDs with Silica-Coated Inorganic Perovskite Quantum Dots. *Adv. Mater.* **2016**, *28*, 10088−10094.
(107) Meyns, M.; Peralvarez, M.; Heuer-Jungemann, A.; Hertog, W.; Ibanez, M.; Nafria, R.; Genc, A.; Arbiol, J.; Kovalenko, M. V.; Carreras, J.; et al. Polymer-Enhanced Stability of Inorganic Perovskite Nanocrystals and Their Application in Color Conversion LEDs. *ACS Appl. Mater. Interfaces* **2016**, *8*, 19579−19586.
(108) Hou, S.; Guo, Y.; Tang, Y.; Quan, Q. Synthesis and Stabilization of Colloidal Perovskite Nanocrystals by Multidentate Polymer Micelles. *ACS Appl. Mater. Interfaces* **2017**, *9*, 18417−18422.
(109) Raja, S. N.; Bekenstein, Y.; Koc, M. A.; Fischer, S.; Zhang, D.; Lin, L.; Ritchie, R. O.; Yang, P.; Alivisatos, A. P. Encapsulation of Perovskite Nanocrystals into Macroscale Polymer Matrices: Enhanced Stability and Polarization. *ACS Appl. Mater. Interfaces* **2016**, *8*, 35523−35533.
(110) Zhang, H.; Wang, X.; Liao, Q.; Xu, Z.; Li, H.; Zheng, L.; Fu, H. Embedding Perovskite Nanocrystals into a Polymer Matrix for

DOI: 10.1021/acsenergylett.7b00547
ACS Energy Lett. 2017, 2, 2071−2083

Tunable Luminescence Probes in Cell Imaging. *Adv. Funct. Mater.* **2017**, *27*, 1604382.
(111) Stoumpos, C. C.; Malliakas, C. D.; Peters, J. A.; Liu, Z.; Sebastian, M.; Im, J.; Chasapis, T. C.; Wibowo, A. C.; Chung, D. Y.; Freeman, A. J.; et al. Crystal Growth of the Perovskite Semiconductor $CsPbBr_3$: A New Material for High-Energy Radiation Detection. *Cryst. Growth Des.* **2013**, *13*, 2722−2727.
(112) Bertolotti, F.; Protesescu, L.; Kovalenko, M. V.; Yakunin, S.; Cervellino, A.; Billinge, S. J. L.; Terban, M. W.; Pedersen, J. S.; Masciocchi, N.; Guagliardi, A. Coherent Nanotwins and Dynamic Disorder in Cesium Lead Halide Perovskite Nanocrystals. *ACS Nano* **2017**, *11*, 3819−3831.
(113) Saliba, M.; Orlandi, S.; Matsui, T.; Aghazada, S.; Cavazzini, M.; Correa-Baena, J.-P.; Gao, P.; Scopelliti, R.; Mosconi, E.; Dahmen, K.-H.; et al. A Molecularly Engineered Hole-Transporting Material for Efficient Perovskite Solar Cells. *Nature Energy* **2016**, *1*, 15017.
(114) Li, X.; Bi, D.; Yi, C.; Decoppet, J. D.; Luo, J.; Zakeeruddin, S. M.; Hagfeldt, A.; Gratzel, M. A Vacuum Flash-Assisted Solution Process for High-Efficiency Large-Area Perovskite Solar Cells. *Science* **2016**, *353*, 58−62.
(115) Cho, K. T.; Paek, S.; Grancini, G.; Roldán-Carmona, C.; Gao, P.; Lee, Y.; Nazeeruddin, M. K. Highly Efficient Perovskite Solar Cells with a Compositionally Engineered Perovskite/Hole Transporting Material Interface. *Energy Environ. Sci.* **2017**, *10*, 621−627.
(116) Choi, H.; Jeong, J.; Kim, H.-B.; Kim, S.; Walker, B.; Kim, G.-H.; Kim, J. Y. Cesium-Doped Methylammonium Lead Iodide Perovskite Light Absorber for Hybrid Solar Cells. *Nano Energy* **2014**, *7*, 80−85.
(117) Saliba, M.; Matsui, T.; Seo, J. Y.; Domanski, K.; Correa-Baena, J. P.; Nazeeruddin, M. K.; Zakeeruddin, S. M.; Tress, W.; Abate, A.; Hagfeldt, A.; et al. Cesium-Containing Triple Cation Perovskite Solar Cells: Improved Stability, Reproducibility and High Efficiency. *Energy Environ. Sci.* **2016**, *9*, 1989−1997.
(118) Balakrishnan, S. K.; Kamat, P. V. Au−$CsPbBr_3$ Hybrid Architecture: Anchoring Gold Nanoparticles on Cubic Perovskite Nanocrystals. *ACS Energy Letters* **2017**, *2*, 88−93.
(119) Linaburg, M. R.; McClure, E. T.; Majher, J. D.; Woodward, P. M. $Cs_{1-x}Rb_xPbCl_3$ and $Cs_{1-x}Rb_xPbBr_3$ Solid Solutions: Understanding Octahedral Tilting in Lead Halide Perovskites. *Chem. Mater.* **2017**, *29*, 3507−3514.
(120) Li, W.; Wang, Z.; Deschler, F.; Gao, S.; Friend, R. H.; Cheetham, A. K. Chemically Diverse and Multifunctional Hybrid Organic−Inorganic Perovskites. *Nat. Rev. Mater.* **2017**, *2*, 16099.
(121) Giustino, F.; Snaith, H. J. Toward Lead-Free Perovskite Solar Cells. *ACS Energy Lett.* **2016**, *1*, 1233−1240.
(122) McCall, K. M.; Stoumpos, C. C.; Kostina, S. S.; Kanatzidis, M. G.; Wessels, B. W. Strong Electron−Phonon Coupling and Self-Trapped Excitons in the Defect Halide Perovskites $A_3M_2I_9$ (A = Cs, Rb; M = Bi, Sb). *Chem. Mater.* **2017**, *29*, 4129−4145.
(123) Volonakis, G.; Filip, M. R.; Haghighirad, A. A.; Sakai, N.; Wenger, B.; Snaith, H. J.; Giustino, F. Lead-Free Halide Double Perovskites via Heterovalent Substitution of Noble Metals. *J. Phys. Chem. Lett.* **2016**, *7*, 1254−1259.
(124) Slavney, A. H.; Hu, T.; Lindenberg, A. M.; Karunadasa, H. I. A Bismuth-Halide Double Perovskite with Long Carrier Recombination Lifetime for Photovoltaic Applications. *J. Am. Chem. Soc.* **2016**, *138*, 2138−2141.
(125) Mir, W. J.; Warankar, A.; Acharya, A.; Das, S.; Mandal, P.; Nag, A. Colloidal Thallium Halide Nanocrystals with Reasonable Luminescence, Carrier Mobility and Diffusion Length. *Chem. Sci.* **2017**, *8*, 4602−4611.
(126) Zhou, C.; Yuan, Z.; Tian, Y.; Lin, H.; Clark, R.; Chen, B.; van de Burgt, L. J.; Wang, J. C.; Hanson, K.; Meisner, Q. J. Highly Luminescent Bulk Quantum Materials Based on Zero-Dimensional Organic Tin Halide Perovskites. *arXiv preprint arXiv:1702.07200*; 2017.
(127) Yang, Y.; Yan, Y.; Yang, M.; Choi, S.; Zhu, K.; Luther, J. M.; Beard, M. C. Low Surface Recombination Velocity in Solution-Grown $CH_3NH_3PbBr_3$ Perovskite Single Crystal. *Nat. Commun.* **2015**, *6*, 7961.

DOI: 10.1021/acsenergylett.7b00547
ACS Energy Lett. 2017, 2, 2071−2083